Measurement Technique for Microwave Surface Resistance of Additive Manufactured Metals

Richard Gumbleton, Jerome A Cuenca, Samuel Hefford, Kenneth Nai and Adrian Porch.

***Abstract*—Additive manufactured (AM) metals are a subject of much interest for their performance in passive microwave applications. However, limitations could arise due to artefacts such as surface texture and/or roughness resulting from the manufacturing process. We have therefore adapted a parallel plate microwave resonator for the accurate measurement of the surface resistance of flat metal plates, allowing for microwave current flow in two orthogonal directions by simply exciting a different resonant mode (at 5.3 and 6.4 GHz), without the need to remove and re-fix the sample. The systematic and random errors associated with the measurement of surface resistance are very small, less than 1% and 0.1%, respectively. The technique is demonstrated with measurements on a range of samples of the alloys AlSi10Mg and Ti6Al4V, manufactured by laser powder bed fusion, in addition to traditionally machined samples of bulk metal alloys of aluminium and brass. For AM samples of AlSi10Mg we have studied the effect on the surface resistance of directional roughness features, generated by the laser raster paths, in directions transverse or parallel to microwave current flow. Importantly for passive microwave device applications, we demonstrate that these samples exhibit no systematic anisotropy of surface resistance associated with such surface features.**

***Index Terms*—Additive manufacture, Parallel Plate, Resonant cavity, Surface resistance.**

I. Introduction

SURFACE resistance (R_S) is a key parameter when assessing the performance of conductive metal surfaces at microwave frequencies. Understanding R_S for a material is important in its optimisation for low-loss microwave applications. In practice the manufacturing process alone will introduce surface features, which have been shown to strongly correlate with microwave loss and hence R_S [1]–[7]. Excess conductor loss associated with surface finish is encompassed within R_S as effective conductivity (σ_{eff}). R_S is defined as

$$R_S = \sqrt{\frac{\pi f \mu_0}{\sigma_{\text{eff}}}} \tag{1}$$

where μ_0 is the permeability of free space (H/m) and f is the operating frequency (Hz). The significance of R_S at microwave frequencies is due to the distributed electrical current within the conductor, with a higher current density near the surface. This phenomenon is known as the skin effect and the depth at which the majority of current is carried is called the skin depth

$$\delta = \sqrt{\frac{1}{\pi f \mu_r \mu_0 \sigma}} \tag{2}$$

where μ_r is the relative permeability. For aluminium alloy AL6082 (of bulk conductivity $\sigma = 2.63\times10^7$ S/m) at a nominal frequency 5.3 GHz, it is calculated that δ = 1.96 μm. Therefore, the majority of current will be carried in the outermost $\approx$ 2 μm of the material which can be of the same scale as micro-surface roughness, leading to a significant impact on power loss. The power dissipated at the conductor surface in the presence of an electromagnetic (EM) field is given by

$$P_c = \frac{R_S}{2}\int_S |H_S|^2 dS \tag{3}$$

where S is the surface on which the current flows (m^2) and H_S is the tangential magnetic field at the metal surface (A/m). This leads to the well-known $\sqrt{f}$ scaling of R_S with frequency, with the effect of surface roughness becoming more apparent as frequency increases (i.e. as the skin depth decreases).

Additive layer manufacturing (ALM) processes have opened up new possibilities for the manufacture of three-dimensional, passive, microwave devices. One example is the powder bed fusion (PBF) process, where layers of atomised metal powder are melted in two-dimensional patterns consecutively, with each layer adding to the three dimensional build. The surface finish can be particularly poor with ALM methods of manufacturing and lead to excess ohmic loss when compared to traditional manufacturing processes [8]. For example, vertical surfaces of PBF samples appear to exhibit higher average microwave loss than equivalent horizontal built samples [9]. This may be explained by the currents crossing layer boundaries, which would be best assessed by forcing current to flow transverse to these boundaries while evaluating for R_S. An application of particular interest for PBF processing is passive waveguide structures, where the current flow patterns are well known and the surface morphology (owing to build orientation) may be optimised for low microwave loss during the design process. Several research studies have used the fabrication of entire waveguide sections and feed-horns to assess the overall microwave performance, often in terms of return loss, of ALM parts [8], [10]–[13]. The relatively good performance of ALM parts shown in these studies is somewhat surprising given the average surface roughness is much higher than in CNC alternatives. Evaluating microwave performance in this way requires large, costly and time consuming sample

Manuscript received June 23, 2020; revised August 24, 2020; accepted September 25, 2020. This work is supported by the Engineering and Physical Sciences Research Council (EPSRC) and Renishaw PLC via an ICASE studentship programme (EP/R511882/1). (*Corresponding author: Richard Gumbleton.*)

R. Gumbleton, S. Hefford and A. Porch are with the School of Engineering, Cardiff University, Queens Buildings, Cardiff, UK, CF24 3AA. (e-mail: gumbletonr1@cardiff.ac.uk).

J.A. Cuenca is with the School of Physics & Astronomy, Cardiff University, Queens Buildings, Cardiff, UK, CF24 3AA.

K. Nai is with the Group Engineering Division at Renishaw PLC, Wotton-Under-Edge, Gloucestershire, UK, GL12 8JR.

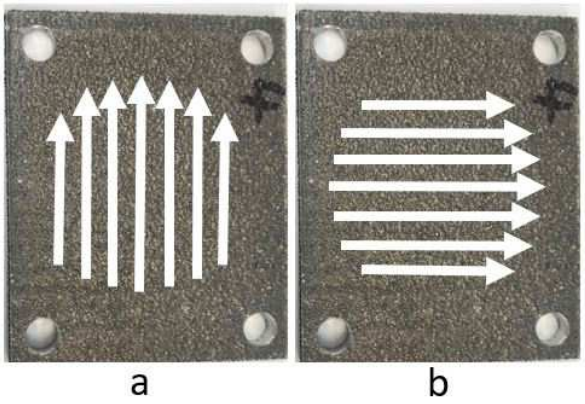

Fig. 1. Schematic representation of induced current flow in additive Manufactured AlSi10Mg samples. The white arrows show the one-dimensional current flow generated through two orthogonal resonant modes of the parallel plate resonator. a) TEM_{001} at 5.3 GHz b) TEM_{010} at 6.4 GHz.

preparation while not allowing for assessment of microwave loss associated with individual surfaces.

Rather than fabricating large samples, several methods for the evaluation of R_S for smaller samples already exist and are represented well in literature. For DC resistance measurements, the conventional four-point-probe method can be highly accurate and fairly simple to use. However, to measure R_S at microwave frequencies two main techniques are established, the 'end wall' replacement of a resonant cavity structure [14] [15] and the use of dielectric resonator (DR) fixtures in various forms [16]–[19]. In the 'end wall' replacement technique, the quality (Q) factor of the TE or TM mode of a cavity resonator (usually manufactured of copper or aluminium) is measured. An end wall is then replaced with a planar sample of the study material and the change in Q factor can be used to extract R_S, relative to that of a reference sample. In the DR fixture approach, a low loss dielectric resonator material (e.g. sapphire) is suspended within a conductive shielding cavity with one wall replaced for the sample. When the dielectric is in close proximity to the sample the loss influence of the sample is greatest. DR fixtures with very high Q factors have been used for measuring superconducting films [20] in addition to a modern lift off DR approach for additive manufactured parts with a high precision [6], [9], [21]. However, in both techniques resonant modes are chosen such that the induced current on the sample only has only azimuthal components [16], [20]. Although appropriate for maximising sensitivity, this means that only isotropic samples can be measured. Owing to the layered nature of ALM parts, and any anisotropy introduced as result of the laser scan pattern used in their production, it would be beneficial to have access to a technique to measure R_S which would enable one-dimensional currents to flow on metal surfaces, and for the current flow direction to be easily rotated by 90 degrees without having to reassemble the fixture.

The aim of this study is to introduce and evaluate an alternative test fixture to enable anisotropy in R_S to be evaluated in flat PBF samples. In our fixture, the use of nearly square samples lead to two resonant modes of similar frequencies,

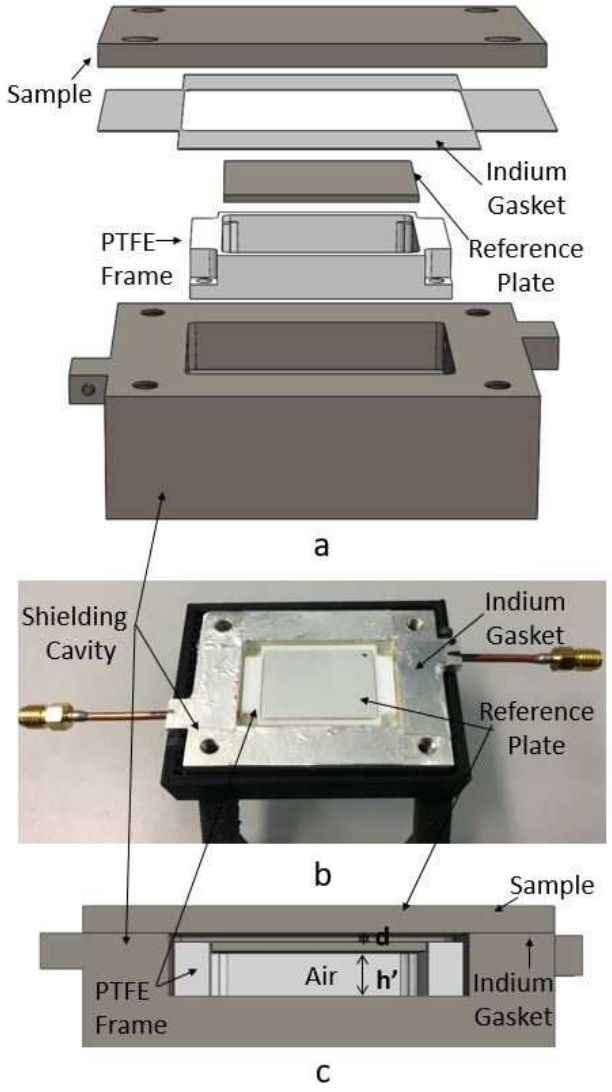

Fig. 2. Enclosed Parallel Plate Resonator. A PTFE frame suspends the small reference plate below the sample within the shielding cavity. Resonant frequency and Q factor are analysed to evaluate R_S of the sample. a) Exploded CAD image, b) Photograph of the Parallel plate resonator, c) CAD Cross section of the assembled fixture.

with orthogonal field patterns and surface currents. The direction of current flow parallel to the sides of the sample is selected by simply altering the frequency of operation, a schematic of this orthogonal current flow is shown in Fig. 1. Since the two frequencies are close, systematic errors linked to an assumed frequency dependence of R_S are minimised. This is done through the adaptation of a parallel plate resonator (PPR), variations of which has been employed in other studies on superconducting materials [22], [23]. These PPR methods used previously involve dielectric spacers sandwiched between superconducting films, which are compressed intimately together through a set of springs external to the cavity. Using our fixture, two discrete frequencies can be excited simultaneously and small ALM sample geometries can be studied without the need for complex compression assemblies. Section II details this methodology, with the derived theory and resonator design of this approach. Section III details a finite element

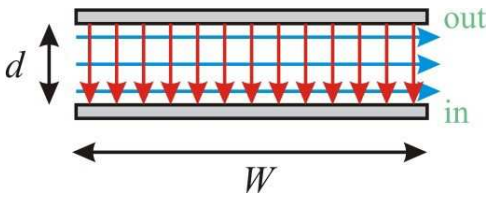

Fig. 3. Schematic diagram showing the idealised, uniform electric (red) and magnetic (blue) fields in the space between the plates of a parallel plate transmission line for the current flow shown (green).

model which is compared to experimental measurements of various metal plates and ALM samples and we draw our final conclusions in Section IV.

II. Measurement Theory

The resonator design is based upon an enclosed parallel plate transmission line structure, where current flows equally on the upper and lower surfaces. In this implementation, the upper surface of the cavity is the sample under test, while the lower surface is formed of a small metal plate held on a PTFE frame. We choose this adaption since then the sample does not need to be cut to a precise size or thickness, it just has to overlap the end of the shielding cavity. Further more, the requirement for screw holes on the sample is not strictly necessary as a simple clamp would ensure the required electrical contact. The metal plate is used as a reference and is common to all measurements, as its dimension fix the resonant frequencies. This means that only the sample is to be replaced, leaving the delicate coupling and metal plate as constants for each measurement. It is possible to include step discontinuities on this plate to excite additional resonant modes [24], however here we focus on the traditional parallel plate geometry. Provided that the walls of the cavity are sufficiently distant to the sample, induced current and hence ohmic loss is equally distributed between the reference plate and the sample, with only minor currents induced in the walls of the host cavity. Measurement of Q factor is used to asses the power loss of the system where, after calibration, differences in measured Q factor can be attributed to R_{S} values and form a comparison between various study samples. A schematic of the enclosed PPR is shown in Fig. 2.

A. Design Equations

1) Resonant Frequency: Simple analytic expressions for resonant frequency and Q factor of the $\mathrm{TEM}_{00\mathrm{p}}$ mode of a PPR can be derived based on the parallel plate transmission line, shown in cross section in Fig. 3. Here, we assume that the current distribution on the cross section is uniform and also that the EM field magnitudes are uniform and contained wholly within the space between the plates (this becoming a better approximation as the aspect ratio d/W tends to zero). The resonance condition is that the line length satisfies $l = p\lambda/2$, where λ is the wavelength along the line and p is an integer (> 0), the longitudinal mode number. The resonant frequencies are then

$$f_0 = \frac{pc}{2\sqrt{\varepsilon_{eff}}l} \tag{4}$$

where $\varepsilon_{\mathrm{eff}}$ is the effective dielectric constant of the line. Although mostly air spaced, the presence of a finite electric field in the PTFE sample frame will cause to be slightly larger than 1, and the fringing fields at the open edges of the parallel plate structure mean that should be replaced by an effective value l_{eff} which is slighly bigger that l owing to the finite plate separation d; the combined effects of $\varepsilon_{\mathrm{eff}}$ and l_{eff} are to reduce f_0 below the simple prediction from Equation 4. The resonant frequencies of the TEM_{001} and TEM_{010} modes of interest in our fixture are then found by replacing l with $b = 25$ mm and $a = 20$ mm, respectively, giving frequencies of 6.0 and 7.5 GHz (in practice reduced to 5.3 and 6.4 GHz, respectively, owing to the effects mentioned above).

2) Q Factor: For a simple analysis of the Q factor, we first consider the conductor Q factor Q_{c}. The resistance per unit length of a parallel plate line is $R \approx 2R_{\mathrm{S}}/W$ so that its conductor attenuation constant is $\alpha_{\mathrm{c}} = R/2Z_0$. Assuming the characteristic impedance is $\mathrm{Z}_0 \approx \eta_0 d/W$ ($\eta_0 \approx 377\ \Omega$ is the free space wave impedance), these results can be combined with Equation 4 to give the following simple expression

$$Q_c = \frac{p\pi}{2\alpha_c l} \approx p\frac{\eta_0}{R_S}\frac{d}{l} \approx 2p\sqrt{\varepsilon_{eff}}\frac{d}{\delta} \tag{5}$$

where $p = 1$ for the TEM_{001} and TEM_{010} modes of interest here. Although greatly simplified, Equation 5 predicts the important dependency that Q_{c} is proportional to the plate separation d but independent of the plate width W. This assumes that the sample plate is parallel to the reference plate [25] and any deviation will change d and hence Q_{c}. In the case of planar metal samples, this error is accounted for during calibration. However for ALM samples, any tilt present may rise from local non-uniform irregularities, quantified by the range in RMS surface roughness ($\mathrm{R_q}$) across the sample. From the ALM samples investigated here, the maximum deviation in $\mathrm{R_q}$ = $\pm$4.5 μm; this could have an effect of raising the quality factor through altering the effective plate separation, leading to an overall underestimate of R_{S} with an error of $\sim 0.45\%$. The dielectric Quality factor Q_{d} is very high since the vast majority of the electric field energy is stored in the air space (by design), but can be written in the usual manner as $Q_{\mathrm{d}} = 1/\tan\delta_{\mathrm{eff}}$, where the effective loss tangent is found from the fraction of stored electrostatic energy U and loss tangent $\tan\delta$ of each component dielectric within the structure.

3) Calibration: Finite element modeling using modern computer simulation package COMSOL Multi-Physics generates very accurate solutions in a non-idealised system such as ours. R_{S} can be found through evaluation of the well known equations for Quality factor [26].

$$Q_T = \omega_0 \frac{\langle U \rangle}{\langle P \rangle} \tag{6}$$

where $\langle U \rangle$ is the time averaged stored energy and $\langle P \rangle$ is the time averaged sum of system losses. Different loss contributors can be isolated through [27]

$$\frac{1}{Q_T} = G_s R_{Ss} + \sum_{m=1}^{i} G_{w_m} R_{Sw_m} + \sum_{p=1}^{j} p_{ed_p} \tan\delta_p \quad (7)$$

where Q_{T} is the total unloaded Q factor of the system, R_{Ss} and G_{s}, R_{Sw} and G_{w} are the surface resistances and geometric values associated with the sample and the summation of i remaining conductive walls of the cavity and sample plate respectively. While p_{ed} is the dielectric filling fraction for j dielectric volumes present in the fixture (e.g PTFE frame and Nylon_{66} screws) . The geometric factors and dielectric filling fractions are defined as

$$G = \frac{1}{\omega} \frac{\iint_s \vec{H}_t \cdot \vec{H}_t^* ds}{\iiint_v \mu_0 \vec{H} \cdot \vec{H}^* dv} \quad (8a)$$

$$p_{ed} = \frac{\iiint_{vd} \varepsilon_{\mathrm{d}} \vec{E} \cdot \vec{E}^* dv}{\iiint_v \varepsilon_{\mathrm{v}} \vec{E} \cdot \vec{E}^* dv} \quad (8b)$$

where s is the surface integral for the conductive surface, v_{d} is the volume integral for the dielectric volume and v is the volume integral for the host cavity. μ_0 is the permeability of free space, and ε_{d} and ε_{v} are the permittivity of the component material and the material filling the cavity respectfully. The numerical value of these geometric factors and dielectric filling fraction will alter for operation in different resonant modes. tanδ is found for the dielectric materials through cavity perturbation while R_{Sw} is found through calibration using a sample of the same material as the cavity walls and reference plate (R_{Sw} = R_{Ss}). This leaves R_{Ss} the only unknown variable from (7) to be analysed when measuring a study sample. Correction for fractional changes in frequency between measurement samples is achieved through

$$R_S(f) \approx Rs(f_0) \times \sqrt{\frac{f}{f_0}} \quad (9a)$$

$$\tan\delta(f) \approx \tan\delta(f_0) \times \frac{f}{f_0} \quad (9b)$$

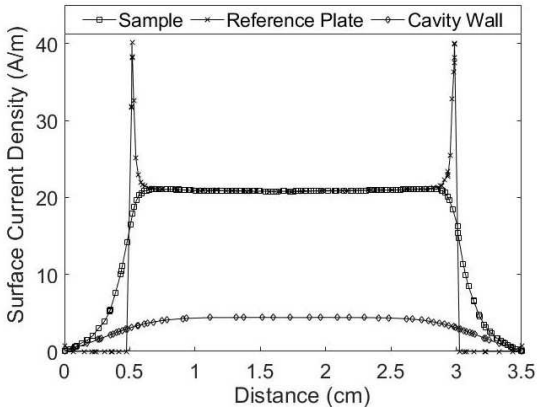

Fig. 4. Simulated surface current density along the length of the cavity. Shown for the surface of the reference plate and surface of the sample, which make a parallel plate resonator. Also shown is surface current density of the cavity wall parallel to the sample. Results are shown for the TEM_{010} resonant mode at 6.4 GHz, where surface currents flow perpendicular to the cut line.

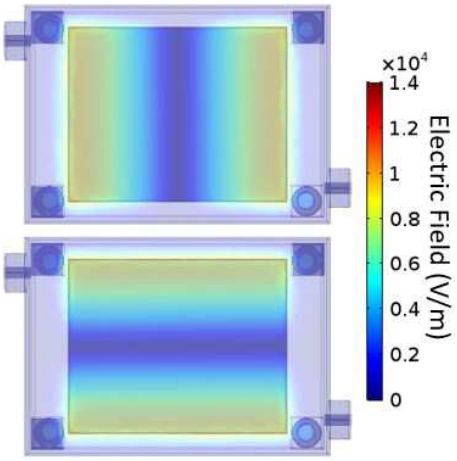

Fig. 5. Top view of the simulated electric field distribution for modes TEM_{001} (Top) at 5.3 GHz and TEM_{010} (Bottom) at 6.4 GHz. The highest concentration of electric field is between the upper surface of the reference plate and the sample.

A final calibration step is performed by measuring a PCB sample (with assumed electrical isotropy) and weighting the results to known values found through an alternative evaluation technique [9]. It should be noted here that this technique is measuring the smooth upper side of the copper PCB cladding rather than the rough bottom side which is usually of significant interest in PCB transmission line applications. This final calibration step is required to account for the current accumulation on the corners of the reference plate, shown in Fig.4. This non-uniform current distribution in the reference plate is constant across all measured samples of different electrical conductivity, so completion of this calibration step is only required once.

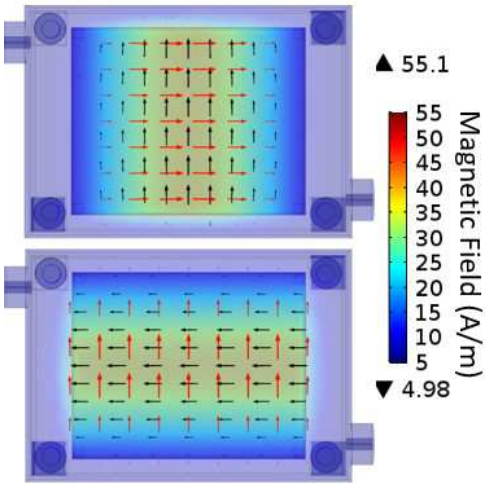

Fig. 6. Top view of simulated induced surface currents (red arrows), magnetic field (black arrows) and magnetic field magnitude for TEM_{001} (Top) at 5.3 GHz where current flow along the length of the sample and TEM_{010} (Bottom) at 6.4 GHz where current flows along its width.

Fig. 7. Cross section of the parallel plate resonator. The color gradient show the electric field (V/m) at the edge of the reference plate. The geometry and placement of the capacitive coupling probe is also shown.

B. Resonator Design

The internal dimensions of the cavity structure are 35 x 25 x 7 mm, while the reference plate is 25 x 20 x 1 mm. This plate is held on a frame of PTFE 1 mm from the surface of the sample. The reference plate and the sample act as a half-wave resonators in both orientations (width and length), with the ratio between length and width being chosen such that sufficient separation of $\sim 20\%$ ($\sim$ 1 GHz) is present between the centre frequencies of the two desired, parallel plate associated, EM resonant modes. It is accepted that when the distance between the lower conducting surface of the reference plate and the lower wall of the host cavity (h') is greater than five times the height of the substrate (d), the loss contribution from the lower wall of the cavity becomes comparatively small [28], as shown in Fig. 4. In addition, the proximity of the side walls of the cavity to the sample must be such as to create a sufficient separation between parallel plate associated modes and cavity associated modes. In doing so also reducing the capacitance between the reference plate and the cavity wall.

In this design the dominant mode of the rectangular cavity TE_{101} is $\sim$ 7 GHz while the half wave resonator frequencies of the reference plate are TEM_{001} at $\sim$ 5.3 GHz and TEM_{010} at $\sim$ 6.4 GHz, owing to the structures rectangular shape. To further increase the influence of the conductors on the total system loss, the traditional dielectric spacer is removed from areas of high electric field, resulting in minimal dielectric loss. The electric field distributions for TEM_{001} and TEM_{010} can be seen in Fig. 5. The corresponding magnetic field induces current flow on the sample. The simulated surface current density and magnetic field distribution for both TEM_{001} and TEM_{010} resonant modes are shown in Fig. 6, where the current on the surface of the sample flows in a uniform pattern, having a directional dependence on the operating mode.

Microwave coupling is achieved through capacitive probes in opposing corners of the cavity volume, as shown in Figs. 5 and 6, orientated parallel to the cavity wall as to align with the electrical field between the sample and reference plate. The coupling probes are placed near the corners of the reference plate in areas of high electric field for both modes of interest and are secured, and grounded, to the shielding cavity by threaded screws clamping the access channel. This placement is chosen to be sufficiently distant as to provide a low coupling coefficient and decrease systematic error. A simulated cross section of the probe geometry and placement is shown in Fig. 7. To ensure a good electrical connection and avoid EM leakage from the fixture, an electrically conductive gasket made of 100 μm thick indium foil (of electrical conductivity (σ) $= 1.2 \times 10^7$ S/m) was placed around the edges of the cavity structure. The extremely pliable metal re-forms to fill the voids between peaks of rough surfaces. This is of particular importance when measuring samples produced of metallic additive manufacturing, where roughness peaks can be $\pm \sim 100$ μm. The gasket enables a good electrical contact with as large of an area of the rough surface as possible, effectively reducing any loss associated with the securing of the sample and maximising the loss contribution from the ohmic properties of the sample itself. This method is presented as a narrow-band approach to assess R_S at two discrete frequencies. To adapt the method for higher activation frequencies, all geometries would need to be miniaturised whilst maintaining the original aspect ratios.

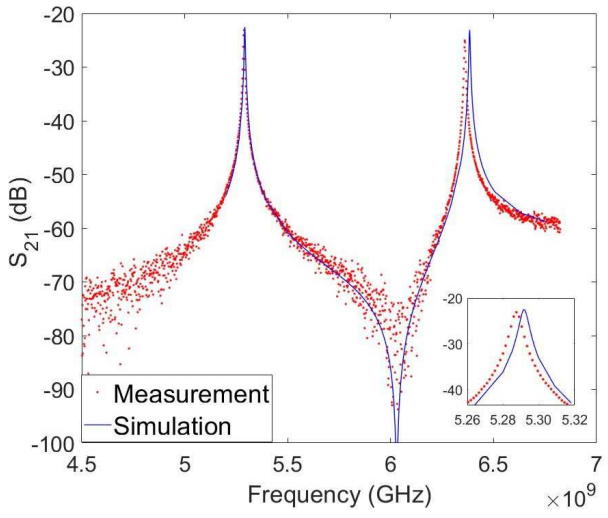

Fig. 8. Graph of S_{21} transmission coefficient for the parallel plate resonator. Red dots are the measured values using a Keysight N5232A PNA. Blue line is the simulated trace using COMSOL multi-physics. Inset is a magnified view of the measured and simulated S_{21} transmission coefficient traces for TEM_{001}.

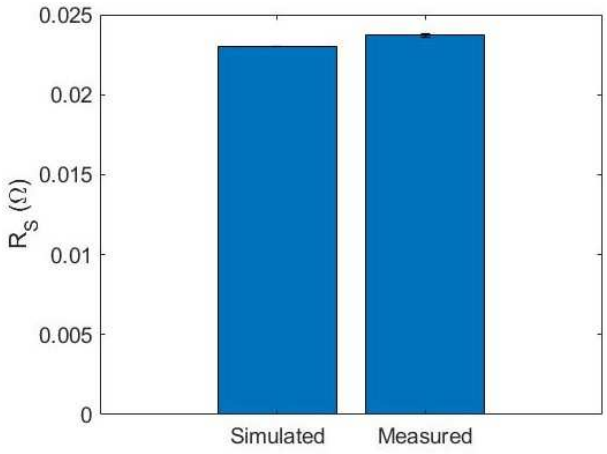

Fig. 9. Chart of simulated and measured surface resistance values for a silver plated aluminium calibration sample, using the silver plated parallel plate resonator fixture in TEM_{010} at 6.4 GHz. Standard error ($\pm 1.9 \times 10^{-4} \Omega$) for 15 measurements is shown via an error bar.

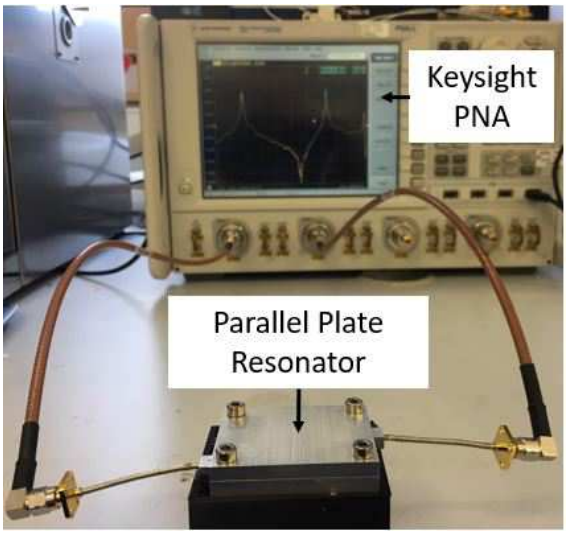

Fig. 10. Photograph of the experimental setup of the parallel plate resonator connected to Keysight N5232A network analyser. Display showing the S21 trace for frequency spanning both resonant modes (TEM_{001} at 5.3 GHz and TEM_{010} at 6.4 GHz).

III. Measurement Results and Discussion

A. Simulation Results

Using COMSOL Multi-physics simulation tool combined with cavity perturbation measurements for ε_r and $\tan\delta$, the loss contribution for each section of the fixture can be evaluated. The parameters used for simulation at 6.4 GHz are: relative permittivity of the PTFE frame (ε_{r_P}) $= 2.09$ and Nylon securing screws (ε_{r_N}) $= 2.70$, dielectric loss for PTFE ($\tan\delta_P$) $= 1.50 \times 10^{-4}$ and Nylon screws ($\tan\delta_N$) = 1.28×10^{-2} and $\sigma = 4.90 \times 10^7$ S/m of the silver plating used on the cavity walls, reference plate and calibration sample. The forward transmission coefficient (S_{21}) traces from both simulation and measurement are shown in Fig. 8 and are in good agreement. Evaluating the field integrals from equations 8a and 8b, and combining with Q_T given through simulation, equation 7 can be solved for R_S. R_S for the silver plated surfaces is determined as $= 23.0$ mΩ at 6.4 GHz. This result compares well with the measured R_S value for the silver plated calibration sample (23.7 mΩ), as shown in Fig.9. The variance in measured R_S for the silver plated calibration sample is 1.2 mΩ over 15 measurements. The loss contributions from each section of the fixture are shown in Table I.

TABLE I
Simulated loss contribution within the parallel plate resonator fixture operating in TEM_{010} mode at 6.4 GHz. Silver plated aluminium is used as the material for the cavity walls, sample and reference plate.

Fixture Section	Loss contribution (%)
Sample	44.06
Reference plate	43.9
Host Cavity Walls	9.62
$Nylon_{66}$ Screws	1.39
PTFE Frame	1.03

B. Experimental Results

Measurements of Q factor were taken for flat metal samples of semi-bright-silver plated aluminium and Rogers Corp. RT/duroid 6002 PCB calibration samples, bulk metal alloys of aluminium AL6082 and brass CZ121 as well as samples produced of AlSi10Mg and Ti6Al4V, by means of PBF. Q factor and frequency were measured through 2-port S-parameters using a lab based, Keysight N5232A network analyser. A photograph of the measurement setup is shown in Fig.10. The transmission coefficient S_{21} is measured with a very small random error, less than 0.1%, due to the high precision of frequency measurement. There is however a larger systematic error associated with the securing and positioning of the sample of $\sim 1\%$ (corresponding to a variation of 14 for a Q factor of 1120 during calibration). Q factor and frequency measurements are evaluated for R_S values through equation 7, using frequency corrected G and p_{ed} from simulation and equations 8a - 9b.

1) Planar Metal Samples: The evaluated R_S values for measured samples can be seen in Fig.11. It is shown that R_S values measured in both resonant modes follow the expected trends when compared to commonly known bulk metal resistivity values, namely that silver and copper PCB exhibit the lowest electrical resistivity ($\sim 1.7 \times10^{-8}$ Ωm) and brass the highest ($\sim 8 \times10^{-8}$ Ωm) out of metals studied here. The standard error for measurements are shown as error bars on Fig.11. For all study samples, R_S is higher in the TEM_{010} mode at 6.4 GHz than in TEM_{001} at 5.3 GHz. This is expected due to the skin effect, where the majority of current is contained in thinner surface layers as frequency increases, and so becomes more susceptible

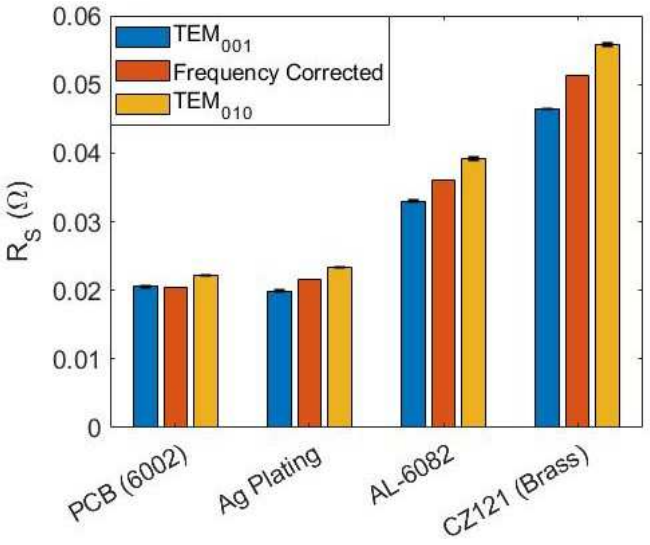

Fig. 11. Surface resistance values of various metal plates. Measurements taken using a parallel plate resonator fixture operating in TEM_{001} at 5.3 GHz and TEM_{010} at 6.4 GHz. Standard error values are shown via error bars, values of which are: in TEM_{001} $\pm4.4\times10^{-5}\Omega$, $\pm1.3\times10^{-4}\Omega$, $\pm1.1\times10^{-4}\Omega$, $\pm8.8\times10^{-5}\Omega$ and in TEM_{010} $\pm4.3\times10^{-5}\Omega$, $\pm8.8\times10^{-5}\Omega$, $\pm2.6\times10^{-4}\Omega$, $\pm1.8\times10^{-4}\Omega$ for Rogers Corp. RT/duroid 6002 PCB, silver plated aluminium, aluminium alloy (AL6082) and brass alloy (CZ121), respectively. Also shown is the frequency corrected R_S values for TEM_{010} scaled down to 5.3 GHz.

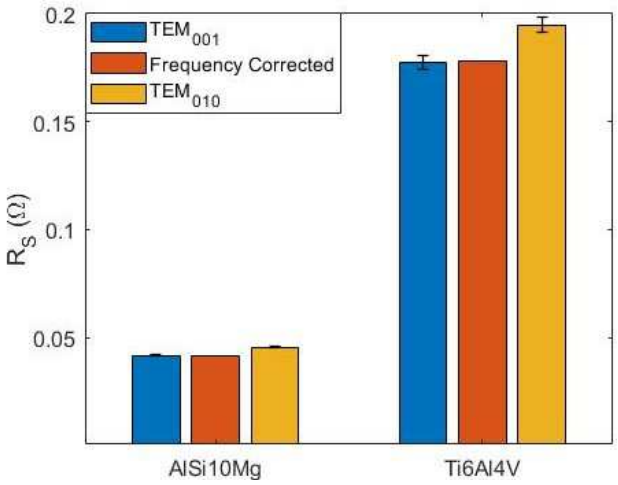

Fig. 12. Surface resistance values for measured samples produced of AlSi10Mg and Ti6Al4V by means of powder bed fusion additive layer manufacturing. Measurements taken using a parallel plate resonator fixture operating in TEM_{001} at 5.3 GHz and TEM_{010} at 6.4 GHz. Standard error values are shown via error bars, values of which are: in TEM_{001} $\pm 2.0\times10^{-4}\Omega$ and $\pm 3.4\times10^{-3}\Omega$, in TEM_{010} $\pm 2.8\times10^{-4}\Omega$ and $\pm 3.5\times10^{-3}\Omega$ for AlSi10Mg and Ti6Al4V, respectively. Also shown is the frequency corrected R_S values for TEM_{010} scaled down to 5.3 GHz.

to loss from micro-surface roughness features. Also shown is the scaled R_S value from 6.4 GHz to 5.3 GHz. This scaled approximation is more closely matched with the value measured in TEM_{001} for Rogers Corp PCB sample, where the surface is expected to be smooth and isotropic. However the increased loss seen at higher frequencies cannot be separated in the bulk metal samples, where machining has introduced micro-surface roughness features / dislocations which might exaggerate loss in the higher frequency mode. Alternatively, the manufacturing process could produce an anisotropic finish on the surface, increasing or reducing R_S in one orientation. Because the induced current flow in the two operating modes flow in orthogonal directions, close matching of values using the simple scaling formula in Eq.9a, can be used to predict isotropic behaviour in R_S of a sample.

2) Additive Manufactured Samples: Samples produced by PBF are evaluated for R_S and shown in Fig.12. As expected,

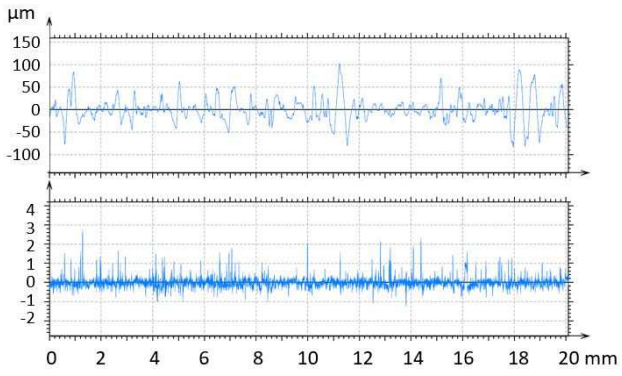

Fig. 13. Roughness profiles of additive manufactured AlSi10Mg (top) and Ag plated aluminium samples bottom. The profiles have been recorded using a Talysurf series 2 drag profiler and analysed with a 0.8mm cutoff filter.

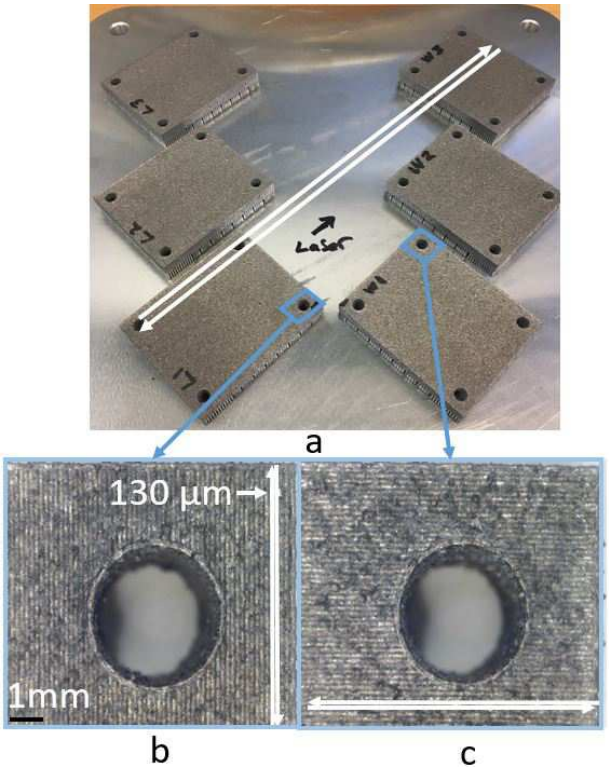

Fig. 14. Photograph of Renishaw AM250 build chamber layout and AlSi10Mg samples produced by powder bed fusion. White arrows indicate the laser raster path. a) Layout for two sample sets so that the laser raster path is across the width or length of the sample. Directional roughness features have been generated along b) the length of the sample and c) the width of the sample.

the R_S value for titanium alloy Ti6Al4V is much higher than that of aluminium alloy AlSi10Mg due to its significantly lower electrical conductivity. The PBF produced aluminium alloy samples showed a slightly larger R_S value than a bulk aluminium alternative (AL6082). The difference between these samples can be ascribed to the excess roughness present from the laser melting process, which has been well documented to increase microwave loss [6], [29], [30]. R_q for the PBF samples were measured as an average of $\sim$ 16.5 μm whilst for the bulk aluminium alloy sample $R_q \approx 0.66$ μm. The roughness profiles shown in Fig. 13 are measured along the length of samples of bulk AL6082 and 'as built' PBF AlSi10Mg using a Talysurf series 2 drag profiler, which have been analysed with a 0.8mm cutoff Gaussian low pass filter. For both AlSi10Mg and Ti6Al4V, the frequency scaled values suggest an isotropic behaviour in terms of R_S. In order to validate this isotropic behaviour, a series of further AlSi10Mg samples were produced, using the laser raster path to generate a directional roughness that is perpendicular to current flow in one mode and parallel to current flow in the other, which are deemed the worse and best cases respectively for microwave loss [4]. Two sets of samples are orientated on the PBF build platform so that each roughness orientation is evaluated in both operating mode. This means that current flow direction can be chosen by changing the mode, not the physical orientation of the samples. The PBF build setup in shown in Fig.14, while using default process parameters for the Renishaw AM250

TABLE II
PROCESS PARAMETERS USED FOR ALSI10MG SAMPLES PRODUCED BY LASER POWDER BED FUSION ON A RENISHAW AM250 ADDITIVE MANUFACTURING SYSTEM.

Laser Power (W)	Hatch Distance (μm)	Layer Thickness (μm)	Exposure Time (μs)	Point Distance (μm)	Laser Diameter (μm)
200	130	25	140	80	70

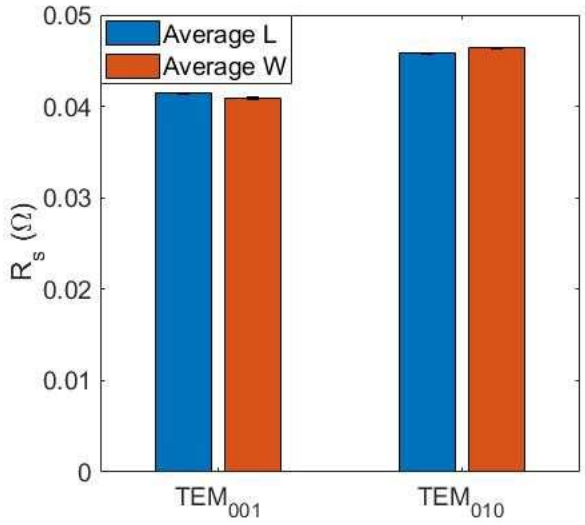

Fig. 15. Average Surface resistance values for AlSi10Mg samples produced with the laser raster path along the length or across the width of the sample. Measurement taken using the parallel plate resonator operating in TEM_{001} mode at 5.3 GHz and TEM_{010} mode at 6.4 GHz. Standard error values are shown via error bars, values of which are: for average L $\pm 6.7\times10^{-5}\Omega$ and $\pm 1.1\times10^{-4}\Omega$, and for average W $\pm 9.8\times10^{-5}\Omega$ and $\pm 6.7\times10^{-5}\Omega$, in TEM_{001} and TEM_{010}, respectively.

additive manufacturing system as shown in Table II. The equivalent scan speed is 512 mm/s using a meander scan pattern. Each layer is orientated at 67^o to the previous layer, with the start angle adjusted such that the laser path for the final layer is parallel to the sample edges. The chamber is vacuumed with a flow of argon to avoid oxidisation of the powder.

The averaged evaluated R_S values for both sample sets are shown in Fig.15. The difference in the averaged values of R_S due to directional roughness features, in both resonant modes, is less than 0.5 mΩ. While the range of R_S values for all samples is $\sim$ 1.5 mΩ. These results suggest that the R_S value, for the PBF surfaces tested, is not dependent on the laser raster path and is effectively isotropic. This explains the perhaps surprisingly good microwave performance of such rough surfaces and has been predicted in a previous, simulated, study into microwave loss in PBF parts [6]. The study predicted that while high R_q values do increase loss compared a perfect flat surface, maximum loss is exhibited when the feature width is $\sim$ three skin depths. For very large or very small feature widths (relative to three skin depths) relatively small increases in loss are observed, compared to ideally flat surfaces. The width of the features produced by the laser raster on the AlSi10Mg PBF samples are large enough, $\approx$ 130 μm, as to be approximated as a near flat surface, given that the skin depths at the operating frequencies is $\approx$ 2 μm.

IV. CONCLUSION

The technique presented in this paper uses a half-wave resonator reference plate, in a enclosed parallel plate fixture, to generate uniform, directional current flow in small study samples. Simultaneously exciting orthogonal resonant modes allows for current flow to be rotated 90 degrees in the study sample, measuring surface resistance in two directions without the need for disassembly, rotation and replacement. Materials investigated using this fixture include bulk metal alloys of aluminium and brass, silver plated aluminium and additive manufactured samples of aluminum and titanium alloys. The measurement results show that this technique is capable of distinguishing between materials of varying electrical resistances with only a small systematic and random error in precision. Additionally, the technique has been shown to be sensitive enough to assess anisotropy in surface resistance for x and y planes of a sample. The effect of laser raster path on surface resistance is also investigated and is shown to be insignificant for horizontal built AlSi10Mg samples.

ACKNOWLEDGMENT

Information on the data underpinning the results presented here, including how to access them, can be found in the Cardiff University data catalogue at http://doi.org/10.17035/d.2020.0113563620.

REFERENCES

[1] E. Hammerstad and O. Jensen, "Accurate models for microstrip computer-aided design," in *Proc. IEEE MTT-S IMS*, Washington, 1980, pp. 407–409.
[2] L. Tsang, X. Gu, and H. Braunisch, "Effects of random rough surface on absorption by conductors at microwave frequencies," *IEEE Microw. Wireless Compon. Lett.*, vol. 16, no. 4, pp. 221–223, 2006.
[3] T. Iwai, D. Mizutani, and M. Tani, "Measurement of high-frequency conductivity affected by conductor surface roughness using dielectric rod resonator method," in *Proc. 2015 IEEE Int. Symp. EMC*, Dresden, 2015, pp. 634–639.
[4] S. P. Morgan, "Effect of surface roughness on eddy current losses at microwave frequencies," *J. Appl. Phys.*, vol. 20, no. 4, pp. 352–362, 1949.
[5] F. Yu and P. Nagy, "Numerical method for calculating the apparent eddy current conductivity loss on randomly rough surfaces," *J. Appl. Phys.*, vol. 95, no. 12, pp. 8340–8351, 2004.
[6] N. Clark, S. Hefford, and A. Porch, "Effects of build orientation and surface finish on surface resistance in microwave components produced by selective laser melting," in *Proc. 47th EuMC*, Nuremberg, 2017, pp. 508–511.
[7] A. Sain and K. L. Melde, "Characterizing the impact of conductor surface roughness on CB-CPW behavior via reduced computational complexity," in *Proc. IEEE 21st Conf. Elect. Perform. Electron. Packag. Syst.*, 2012, pp. 260–263.
[8] P. Booth and E. Valles Lluch, "Enhancing the performance of waveguide filters using additive manufacturing," *Proc. IEEE*, vol. 105, no. 4, pp. 613–619, 2017.
[9] R. Gumbleton, S. Hefford, K. Nai, and A. Porch, "Effects of post-processing treatments on the microwave performance of additively manufactured samples," in *Proc. 13th Eur. Conf. on Antennas Propag.*, Krakow, 2019.

[10] M. Kilian, A. Schinagl-Weiß, A. Sommer, C. Hartwabger, and M. Schneider, "Ku-band SFB-cluster manufactured by additive manufacturing techniques," in *Proc. 13th Eur. Conf. Antennas Propag.*, Krakow, 2019.
[11] O. Peverini et al., "Selective laser melting manufacturing of microwave waveguide devices," *Proc. IEEE*, vol. 105, no. 4, pp. 620–631, 2017.
[12] O. Addamo et al., "Experimental research activity on additive manufacturing of microwave passive waveguide components," in *Proc. 47th EuMC*, Nuremberg, 2017, pp. 496–499.
[13] M. Hollenbeck, K. Wamick, C. Cathey, J. Opra, and R. Smith, "Selective laser melting aluminum waveguide attenuation at K-band," in *Proc. IEEE MTT-S IMS*, Honololu, 2017, pp. 45–47.
[14] B. A. Tonkin and Y. G. Proykova, "Microwave surface resistance of cuprate superconductors," *IEEE Trans. Appl. Supercond.*, vol. 7, no. 2, pp. 1257–1259, 1997.
[15] D. Cooke et al, "Surface resistance of $YBa_2Cu_3O_7$ films deposited on $LaGaO_3$ substrates," *Appl. Phys.*, vol. 55, no. 9, pp. 914–916, 1989.
[16] M. J. Lancaster, *Passive Microwave Device Applications of High-Temperature Superconductors*. Cambridge University Press, 1997.
[17] R. Fletcher and J. Cook, "Measurement of surface impedance versus temperature using a generalized sapphire resonator technique," *Rev. Sci. Instrum.*, vol. 65, no. 8, pp. 2658–2666, 1994.
[18] J. Mazierska and C. Wilker, "Accuracy issues in the surface resistance measurements of high temperature superconductors using dielectric resonators," *IEEE Trans. Appl. Supercond.*, vol. 11, no. 4, pp. 4140–4147, 2001.
[19] B. Hakki and P. Coleman, "A dielectric resonator method of measuring inductive capacities in the millimeter range," *IEEE Trans. Microw. Theory Techn.*, vol. 8, no. 4, pp. 402–410, 1960.
[20] J. Krupka and J. Mazierska, "Improvement of accuracy in measurements of the surface resistance of superconductors using dielectric resonators," *IEEE Trans. Appl. Supercond.*, vol. 8, no. 4, pp. 164–167, 1998.
[21] S. Hefford, N. Clark, R. Gumbleton, and A. Porch, "Lift-off dielectric resonator for the microwave surface resistance measurement of metal plates," *Under Review*, 2020.
[22] S. A. Reible and C. W. Wilker, "Parallel plate resonator for accurate RF surafce loss measurements," *IEEE Trans. Magn.*, vol. 27, no. 2, pp. 2813–2816, 1991.
[23] R. C. Taber, "A parallel plate resonator technique for microwave loss measurements on superconductors," *Rev. Sci. Instrum.*, vol. 61, no. 8, pp. 2200–2206, 1990.
[24] C. Railton and T. Rozzi, "The rigorous analysis of cascaded step discontinuities in microstrip," *IEEE Trans. Microw. Theory Techn.*, vol. 36, no. 7, pp. 1177–1185, 1988.
[25] C. A. Valagiannopoulos and N. K. Uzunoglu, "Rigorous computation of green's function of a parallel-plate waveguide with a tapered wall," *Electromagnetics*, vol. 29, no. 3, pp. 203–219, 2009.
[26] D. Pozar, *Microwave Engineering*, 4th ed. Wiley, 1998.
[27] S. Hefford, "Microwave processing in additive manufacturing," PhD Thesis, Cardiff University, 2019.
[28] K. C. Gupta, R. Garg, I. Bahl, and P. Bhartia, *Microstrip Lines and Slotlines*. Artech House, 1996.
[29] B. Zhang et al, "Metallic 3-D printed antennas for millimeter- and submillimeter wave applications," *IEEE Trans. THz Sci. Technol.*, vol. 6, no. 4, pp. 592–600, 2016.
[30] J. A. Lorente, M. M. Mendoza, A. Z. Petersson, L. Pambaguian, A. A. Melcon, and C. Ernst, "Single part microwave filters made from selective laser melting," in *Proc. 2009 EuMC*, Rome, 2009, pp. 1421–1424.

Richard Gumbleton received the B.Eng. (Honours) degree in electronic and communications engineering from Cardiff University, U.K., in 2017. He is currently working towards the Ph.D. degree in Microwave Engineering, also at Cardiff University as part of an ICASE studentship award with Renishaw PLC. His research interests include additive manufacturing for microwave applications, specifically the characterisation and optimisation of additive manufactured surfaces.

Jerome Cuenca received the B.Eng. (Honours) in electronic and communications engineering from Cardiff University, U.K., in 2012 and Ph.D. in microwave materials science 2015. He is currently at the Cardiff Diamond Foundry, School of Physics, Cardiff University, U.K. His research focuses on microwave dielectric spectroscopy of various materials and microwave plasma assisted chemical vapour deposition of diamond.

Samual Hefford received the B.Eng. (Hons.) degree in Electronic and Communications Engineering and PhD degree in Microwave Engineering from Cardiff University, UK. His research utilises microwave resonant structures and involves the development of measurement and processing techniques for metal powder compacts and additive surfaces. He currently works as a research associate at Cardiff University in the Centre for High-Frequency Engineering.

Kenneth Nai received the B.Sc. (Honours) degree (First Class) in Electronics and Electrical Engineering and Ph.D. degree in Control Systems from Loughborough University, U.K., in 1990 and 1995 respectively. He has been in employment with Renishaw PLC, U.K. since 1995 and is currently a Principal Engineer, where he has developed products in the field of metrology systems, Neuro-surgical Robotics and Metal Powder 3-D printers. He is a Chartered Engineer, a Member of the Institution of Engineering and Technology, and has been granted 12 U.S. Patents.

Adrian Porch received the M.A. degree in physics and the Ph.D. degree in low temperature physics from Cambridge University, Cambridge, U.K. He is currently a Professor with the School of Engineering, Cardiff University, Cardiff, U.K., where he leads the Center for High Frequency Engineering. He has 34 years of experience in applying microwave methods to measure and understand the fundamental properties of electronic materials, with 165 relevant publications. More recently he has developed microwave sensors and applicators across different disciplines, including new medical sensors and new methods in electron paramagnetic resonance spectroscopy.